Light Metals 2011 *Edited by: Stephen J. Lindsay*
TMS (The Minerals, Metals & Materials Society), 2011

ALUMINATE SPINELS AS SIDEWALL LININGS FOR ALUMINUM SMELTERS

X. Y. Yan[1], R. Z. Mukhlis[2], M. A. Rhamdhani[2], and G. A. Brooks[2]
[1]CSIRO PSE, Box 312, Clayton South, Victoria 3169, Australia
[2]Swinburne University of Technology, PO Box 218, Hawthorn, Victoria 3122, Australia

Keywords: aluminate spinel, sidewall, corrosion behavior

Abstract

Ledge-free sidewall is preferred as it potentially reduces the energy requirement of aluminium production by about 30%. However, this approach poses great material challenges because such sidewalls are in direct contact with oxidizing, corrosive and reducing environments at different cell locations. In this study, $NiAl_2O_4$, $MgAl_2O_4$ and $Ni_{0.5}Mg_{0.5}Al_2O_4$, were identified and tested in cryolite-AlF_3-Al_2O_3-CaF_2 electrolyte melts at 980 °C under air and CO_2. Both specimens and baths were characterized using XRD, XRF and SEM-EDS methods. This study revealed that the $NiAl_2O_4$ and $MgAl_2O_4$ spinels had good corrosion resistance toward the melts under CO_2, with solubility of Ni from $NiAl_2O_4$ being 0.01wt% and Mg from $MgAl_2O_4$ being 0.07wt%. Dissolution of Ni and Mg into the bath was lowered to 0.007wt% Ni and 0.05wt% Mg through the formation of a $Ni_{0.5}Mg_{0.5}Al_2O_4$ solid solution.

Introduction

Aluminum is commercially produced in the Hall-Héroult cells (HHC). The HHC consists of a steel shell lined with refractory insulating bricks covered with sidewall lining materials, a pool of molten Al on carbon blocks as the cathode at the bottom of the cell, and a carbon block immersed in the electrolyte from the top of the cell as the anode. Molten Al is produced at the cathode while the carbon anode is electrochemically oxidised and, thus, consumed during electrolysis to produce 70-90% CO_2, with the rest being CO [1]. The overall cell reaction can be expressed as:

$$2\ Al_2O_3\ (diss) + 3\ C\ (s) = 4\ Al\ (l) + 3\ CO_2\ (g) \qquad (1)$$

The reversible cell voltage is 1.19 V at a typical electrolysis temperature of 960 °C. Modern HH standard cells today operate at up to 380-400 kA, with the first commercial AP50 line being built (the trial cells require 13.25 kWh/kg Al at 500 kA amperage and 95.7% current efficiency) [2].

In practice, cell sidewalls are covered by a layer of a solidified electrolyte normally termed side ledge or side freeze which protects the side linings from a corrosive cryolite-based electrolyte melt (bath) and a highly reducing molten Al. Either service life of the sidewall materials or the carbon cathode may be the limiting factor in overall cell life, depending on the individual materials employed and operating practice applied. There have been significant advances in enhancing energy efficiency and productivity and reducing greenhouse gas emissions over the past 60 years [3-9]. Noticeably, emerging technologies being developed for the HH process would lead to changes in heat balance within the cell, with the amount of heat dissipated through the sidewalls likely to be lowered [3, 10]. Hence, novel sidewall designs and associated materials stable towards surrounding environments are essential to commercialization of the above technologies.

Carbon blocks are traditionally used as sidewall linings in the HHC [1]. Recently, Si_3N_4-bonded SiC refractory has been increasingly utilized as the lining materials since it can (i) extend cell life through improved oxidation and cryolite resistances, (ii) increase cell capacity and (iii) facilitate application of large-sized anodes to the cells, thereby leading to an overall increase in cell productivity [1,8,11-12]. However, Si_3N_4-bonded SiC refractories have higher manufacturing costs than carbon blocks. There are intrinsic problems associated with the HHC when the carbon and Si_3N_4-bonded SiC sidewall linings are unprotected by a side ledge. The problematic issues for un-protected carbon blocks mainly include reactions with O_2 or CO/CO_2 dissolved in baths, bath penetration, chemical erosion due to Al_4C_3 formation, spalling due to Na intercalation, mechanical abrasion due to undissolved Al_2O_3 particles in circulation and easier erosion at metal/bath/carbon three phase boundaries [1]. For un-protected Si_3N_4-bonded SiC, the problems are dissolution of Si_3N_4 in baths and chemical reduction of SiC by liquid Al [13, 14]. Current practice to minimize these sidewall attacks is to operate the HHC with the side ledge by ensuring that heat loss through the sidewall is carefully balanced, thereby maintaining stable side ledge formation. Such a heat loss due to this practice accounts for approximately 30-40% of the total energy consumption, which is largely responsible for 40-45% energy efficiency of the current HH process [3].

The downside of the side ledge is that there are occasions where the sidewall may be exposed to a molten bath in the HHC. For example, during cell start-up, the molten bath will be in direct contact with the sidewall lining for a period of time before the formation of a protective side ledge. In other occasions, the protective side ledge may melt away during anode effects or cell instability. In both instances the sidewall is directly exposed to the bath, causing potential degradation and/or sidewall failure. An alternative approach of tackling these difficulties is to develop a sidewall that does not require a side ledge to protect such attacks, i.e., a ledge-free sidewall where the lining is directly exposed to the surroundings during cell operations. With such a ledge-free sidewall, the heat within the HHC needs to be kept rather than removed. This leads to a potentially 30-40% energy savings that would otherwise be lost through the sidewalls with a side ledge. Furthermore, the cell capacity and productivity may be most increased with a ledge-free sidewall cell configuration. Despite these obvious benefits, few efforts have been so far made to develop the sidewall materials that enable the HHC to operate in aggressive ledge-free cell operating environments.

Ultimate Materials Challenge and Opportunity

One of the primary obstacles to the ledge-free sidewall approach is a lack of suitably refractory sidewall materials that are able to withstand all different surrounding environments [1, 3, 15]. Thus, the approach poses substantial materials challenge. On the other hand, the discovery of material that could serve as a ledge-free sidewall, especially if combined with inert anodes and a wettable cathode, would enable major changes in cell design and operating practice. This would improve energy utilization and reduce environmental impacts. Welch and May [15] and Pawlek [16] have summarized general selection criteria for an ideal sidewall material after considering physical, chemical, and economical requirements, as given in Table I.

Table I. General selection criteria of sidewall refractories for use in Al electrolysis cells [15, 16].

Physical	High electrical resistivity
	High thermal conductivity
	Superior abrasion resistance to sludge
	High mechanical strength
Chemical	Not reactive to cryolite
	Not reactive to molten Al and Na
	Insoluble in molten cryolite and Al
	Not oxidised by air
	Impervious or low porosity
	Not wetted by bath or metal
Economical	Low fabrication costs, and
	Ease of joining

To date, no single material has been identified that can satisfy all the chemical requirements in Table I. The efforts have focused on carbon based and non-oxide ceramic based materials, whereas the use of oxide based ceramics as ledge-free sidewall materials has not been fully explored largely because most oxides exhibit unacceptable high solubilities in HH baths [16-18]. There are, however, certain oxides or complex oxides that can provide acceptably high chemical stability towards the baths, typically those currently under investigation for the development of cermet inert anodes in the HHC [6, 19]. The recent study further shows that $NiFe_2O_4$ exhibited a limited solubility in molten cryolite-AlF_3-CaF_2-Al_2O_3 electrolytes at 1000 °C, especially when the melts contained high contents of Al_2O_3 and atmospheres of the cell had high oxygen potentials, and it could be readily prepared from cheap NiO and Fe_2O_3 thus resulting in a potential cost reduction in refractory fabrications compared to those of Si_3N_4-bonded SiC [20]. Hence, opportunities exist for oxide based ceramics as sidewall materials in the HHC.

In the present study, we propose a series of aluminate spinels, including $NiAl_2O_4$, $MgAl_2O_4$ and $Ni_xMg_{(1-x)}Al_2O_4$ solid solutions, as candidate materials for use as the sidewall linings in the HHC and present a set of preliminary experimental results to demonstrate their chemical stabilities towards molten cryolite-AlF_3-CaF_2-Al_2O_3 electrolytes at 980 °C. Provided that the selected spinels also fulfill the other requirements in Table I except for thermal conductivity, the application of the spinel-type sidewall materials to the HHC may potentially lead to a novel design of the sidewall where no side ledge is required.

Thermodynamic Analysis

Equilibrium calculations on the systems $MgAl_2O_4$, $NiAl_2O_4$, and $NiFe_2O_4$ with molten aluminium and electrolyte bath were carried out using FactSage 6.1 thermodynamic package using FTlite, FThall and FToxid solution models and databases [22]. The liquid solution phase in FTlite (light metal database) uses modified quasichemical model taking into account short range ordering tendency of atoms or molecules in liquid solutions. The solid solutions of spinel and monoxide in FToxid (oxide database) takes into account the mixing of various cations on crystallographically different sublattices. The cryolite bath model in the FThall assumes a non-random mixing of elemental cations and anions on their respective sublattices [22]. All calculations were carried out for the temperature range of 900 to 1010 °C using the parameters used in the experimental part (e.g. the amount and composition of spinel, aluminum and electrolyte bath).

Figure 1 show the predicted equilibrium solute concentrations of Mg and Ni in molten aluminum when 6 g of each spinel ($MgAl_2O_4$, $NiAl_2O_4$, and $NiFe_2O_4$) is reacted with 224 g aluminum. In the case of $MgAl_2O_4$, the predicted Mg equilibrium concentration in aluminum increased from 0.057 to 0.094 wt% as the temperature was increased. In the case of $NiAl_2O_4$ and $NiFe_2O_4$, the nickel concentration in the aluminum was predicted to be constant, as all nickel dissolved in aluminum at all temperature studied. It should be noted that for the same sample mass, the amount of nickel dissolved from $NiFe_2O_4$ sample was lower than that of from $NiAl_2O_4$ sample. This is because, for the same amount sample mass, $NiFe_2O_4$ brings less Ni into Al melt than $NiAl_2O_4$, if Ni is completely dissolved into Al melt. These results indicate that in molten aluminum; $MgAl_2O_4$ is more stable compared to $NiAl_2O_4$ and $NiFe_2O_4$. Worth to be mentioned that the the typical concentration ranges of impurity elements in primary aluminium metal is 1-80 ppm Ni, 5-60 ppm Mg and 400-3000 ppm Fe [23].

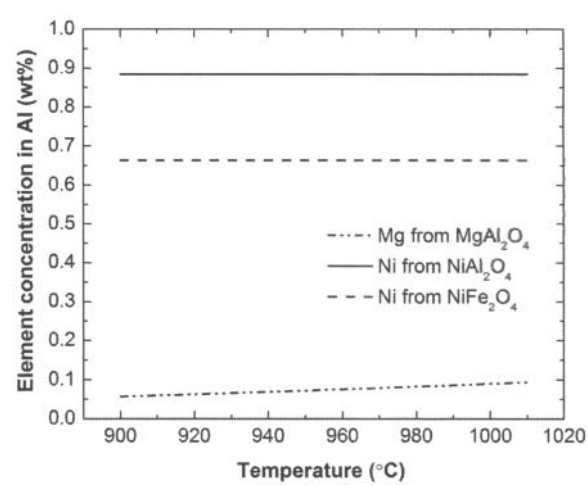

Figure 1. Predicted equilibrium concentration of Mg and Ni in aluminum when 6 g of each spinel ($MgAl_2O_4$, $NiAl_2O_4$ and $NiFe_2O_4$) is reacted with 224 g liquid aluminum.

In the case of equilibrium between $MgAl_2O_4$ and electrolyte bath system, $MgAl_2O_4$ was predicted to be unstable in the given temperature range, as all spinel was dissolved in the cryolite. Figure 2(a) shows the predicted equilibrium Mg content and

concentration in the electrolyte bath. All Mg (~1.03 g) in the spinel was predicted to be dissolved in the bath. The change in Mg concentration in the bath shown in Figure 2(a) was due to the change in the amount of liquid bath due to the dissolutions of other solid phases such as Na_3AlF_6(s) and Al_2O_3(s). This can be seen clearly in Figure 2(b) that shows the equilibrium amount of various phases. At 900 °C, more than half of the cryolite (about 169.6 g) was in the form of solid which decreased as temperature was increased. The cryolite was completely dissolved at 950 °C.

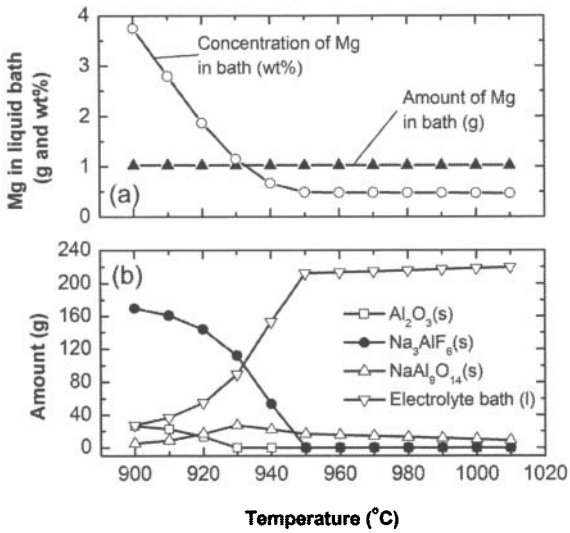

Figure 2. (a) Predicted equilibrium amount and concentration of Mg in electrolyte bath; (b) equilibrium amount of phases when 6g of $MgAl_2O_4$ is reacted with 200g cryolite and 22g Al_2O_3.

The current liquid bath solution models in FThall in FactSage do not take into account nickel. For this reason, in the case of $NiAl_2O_4$ and $NiFe_2O_4$ in electrolyte bath, the Ni concentration in the bath was evaluated using the nickel solubility equation reported by Lorentsen [24]:

$$wt\%Ni^{2+} = -0.0755 + \left[\frac{0.27896}{x^{1/2}}\right] \quad (2)$$

where x is the amount of alumina in wt% (from 0.9 to 13.1 wt%). Using this equation, the solubility of nickel in the bath, containing 10 wt% alumina, was calculated to be 0.013 wt%. For 6g of $NiAl_2O_4$ and $NiFe_2O_4$ immersed in 22 g alumina and 200 g cryolite, the total amount of nickel in the system was calculated to be 0.0087 and 0.0066 wt%, respectively. These amounts are smaller than the solubility limit. Therefore (from thermodynamic point of view), it may be that all nickel from the $NiAl_2O_4$ and $NiFe_2O_4$ dissolve into the bath. It should be emphasized, however, that the above analyses consider thermodynamic factor only but does not consider critical kinetic factors and thus provide the theoretical limits.

Experimental

The NiO powder used had a mean particle size of 10 μm, with 76-77% Ni. The MgO powder was 98-100% pure on ignited material. The Fe_2O_3 powder was at least 99% pure, with mean particle sizes less than 5 μm. The Al_2O_3 powder was 99.7% pure and had particle sizes less than 10 μm. The AlF_3 and CaF_2 used were analytical reagents. The as-purchased synthetic cryolite powder contained at least 96.5% Na_3AlF_6 and approximately 1% CaF_2 and 2% Al_2O_3 with the rest being $Na_5Al_3F_{14}$, as determined using standard X-ray fluorescence spectroscopy (XRF) and X-ray diffraction (XRD) techniques.

To fabricate pure oxide spinels, the oxide precursors were weighed at stoichiometric ratios corresponding to individual oxide spinels. The weighed mixture was ball milled in acetone for 24 h and dried in air. Approximately 14g of the thoroughly mixed oxides were cold-pressed in hard steel dies into a rectangular bar under a uniaxial pressure of 120 MPa. Green bars were then sintered in air at 1500 °C for 3-72 h. To prepare a spinel solid solution, the prepared pure oxide spinels were crushed and ground for 10 min into powders. The two powders were weighed at a desired mass ratio and mixed completely. The well mixed pure spinel powders were pressed into a green rectangular bar under 120 MPa. The green bar was sintered in air at 1500 °C for 72 h. The dimension of each sintered bar was about 45 mm long, 12 mm wide and 6 mm thick.

The methods of immersion-type and stirred finger tests were utilized in this work. In an immersion-type test, one test specimen was fully immersed in a molten bath at 980 °C for a given period, during which the bath was sampled at various intervals. The samples taken were analyzed for elemental concentrations. Details of the stirred finger tests have been described previously [20]. In the stirred finger test method, one end of the sintered bar was assembled into a stainless steel holder and an outer surface of the holder was covered with an alumina tube. Space gaps between the holder and the tube were then filled with alumina cement to ensure that the complete holder surface was not directly exposed to molten bath during testing. The bar to be tested was immersed in the molten bath and rotated at a pre-determined rotation speed for a given period of time at 980 °C. The rotation speed was chosen so that the concentrations of dissolved elements from the bar were independent of distances from the sample surface, i.e., the mass transfer was not a rate-determining step in controlling the overall dissolution rate. Under such conditions, the concentrations of the dissolved elements from the bar in the bath are regarded as the solubility of the material in the bath at 980 °C.

After testing, solidified baths were crushed and ground into powders and tested specimens were mounted and sectioned. Both were then examined to determine the extents of reaction. Phases of the specimens and bath samples were identified by XRD. Microstructures and elemental concentrations of the specimens were examined using the scanning electron microscopy (SEM) with an energy dispersive spectrum (EDS). Elemental concentrations of the bath samples were analyzed by XRF.

Results and Discussion

The aluminate spinels tested were $NiAl_2O_4$, $MgAl_2O_4$ and $Ni_{0.5}Mg_{0.5}Al_2O_4$, with Ni and Mg ferrite spinels also tested for comparison. The experimental conditions used for preparation and bath tests of the spinel specimens are given in Table II.

Characterization of prepared test specimens

The X-ray diffraction experiments have been performed on a Bruker AXS D8 diffractometer using the Cu Kα radiation

(λ = 0.15406 nm). The scattering intensities were measured over an angular range of $5° < 2\theta < 80°$ with a step size $\Delta(2\theta)$ of 0.02° and a scan speed of 0.8°/min. The result of XRD performed on the sintered oxide precursors powder confirmed that only spinel phase exist in the powder as shown in Figure 3. No other phases were evident from the diffraction pattern. The lattice parameter of the $NiAl_2O_4$, $MgAl_2O_4$ and $Ni_{0.5}Mg_{0.5}Al_2O_4$ in Figure 3 was calculated to be 8.048, 8.083 and 8.0836 Å, respectively.

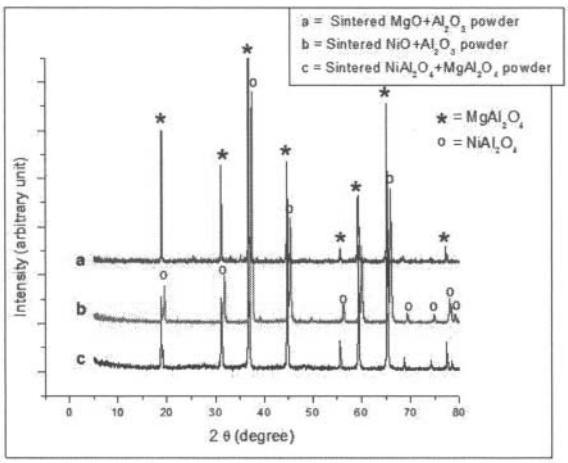

Figure 3. XRD pattern of sintered oxide precursor powders

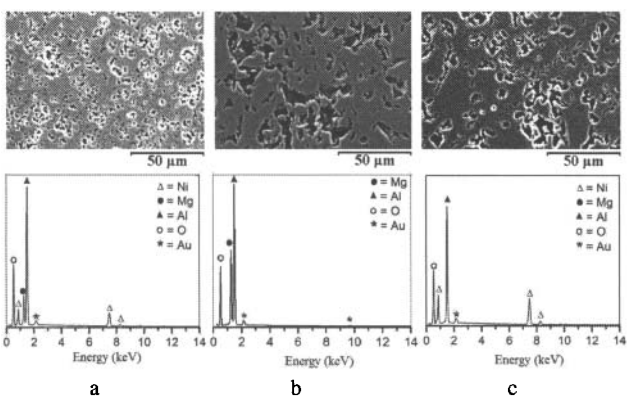

Figure 4. SEM micrographs and the associated EDS result of as prepared (a) $NiAl_2O_4$, (b) $MgAl_2O_4$, and (c) $Ni_{0.5}Mg_{0.5}Al_2O_4$ samples

The SEM micrographs in Figure 4 show that the bar samples contain significant porosity. Large and interconnected pores may accommodate bath to penetrate deep into the sample. On the other hand, very dense sample is also not favorable as it tends to easily broken during a thermal cycle. It should be noted that microstructure optimization was not performed in present work. Currently, the spinel microstructure optimization is being carried out by PYROmetallurgical Group at University of Wollongong. According to the energy dispersive spectroscopy, the content of Al and Ni in $NiAl_2O_4$ sample is 26.02 and 12.80 at%, respectively. $MgAl_2O_4$ contains 11.86 at% Mg and 23.40 at% Al. $Ni_{0.5}Mg_{0.5}Al_2O_4$ sample contains 5.95 at% Mg, 6.23 at% Ni and 25.39 at% Al. Associated with the XRD results; the EDS results also appear to indicate that spinel structure has been formed in the samples as the relative at% ratio of metallic elements in the samples are very close to the desired stoichiometry ratio of elements of the target spinels.

Chemical interactions

The interactions between aluminate or ferrite spinels and molten cryolite-AlF_3-CaF_2-Al_2O_3 electrolytes may involve: (i) chemical reactions between component oxides from the spinels and the electrolytes and (ii) dissolution reactions. At Al_2O_3 concentrations greater than 5 wt%, the dissolution reactions are mainly expressed as follows [20]:

$$3\ MAl_2O_4\ (s) + 2\ (AlF_3) = 3\ (MF_2) + 4\ (Al_2O_3) \quad (2)$$

$$3\ MFe_2O_4\ (s) + 8\ (AlF_3) = 3\ (MF_2) + 6\ (FeF_3) + 4\ (Al_2O_3) \quad (3)$$

where M = Ni or Mg. Reactions 2 and 3 imply that Ni and Mg from the spinels dissolve into the electrolyte melts to form respective metal fluorides. Fe from the ferrite spinels also dissolves into the melts. Reactions 2 and 3 can be shifted towards the left by increasing activities of Al_2O_3 dissolved in the melts at given temperatures. Dissolution behaviors of the prepared spinels were investigated experimentally under the conditions in Table II.

Table II shows the measured concentrations of elemental Al, Ni, Mg, Fe and Ca dissolved in the Al_2O_3-saturated cryolite-AlF_3-CaF_2-Al_2O_3 melts after bath tests of $NiAl_2O_4$, $MgAl_2O_4$, $Ni_{0.5}Mg_{0.5}Al_2O_4$, and $NiFe_2O_4$ under CO_2 at 980 °C. It was found that Ni concentrations in the melt in contact with the $NiAl_2O_4$ specimen stabilized at 0.01 wt% Ni after 30-hours immersion test. This value was much lower than measured for the $NiFe_2O_4$ spinel (0.045 wt% Ni). However, it was slightly higher than the concentration of Ni (0.0027-0.004 wt% Ni) in an Al_2O_3-saturated cryolite-Al_2O_3 melt in equilibrium with solid $NiAl_2O_4$ and Al_2O_3 at 980 °C measured by Jentoftsen *et al.* [25]. This observed higher Ni content can largely ascribed to the presence of CaF_2 in the present bath. The XRF results indicated that the $NiAl_2O_4$ was chemically more stable than $NiFe_2O_4$ in terms of dissolution of Ni from the spinels in the melts at 980 °C.

It was also found that the concentration of Mg from the $MgAl_2O_4$ was 0.07 wt% Mg after 151.12-hours immersion test in the melt in contact with the $MgAl_2O_4$, which was seven times higher than that of Ni from the $NiAl_2O_4$ under the same test conditions but was at least five times lower than that of Mg from the $MgFe_2O_4$ tested at the bath ratio of 1.5 under air. It was interesting to note that the concentrations of Ni and Mg from the $Ni_{0.5}Mg_{0.5}Al_2O_4$ solid solution in the bath were lowered to 0.007 wt% Ni and 0.05 wt% Mg due to reduced activities of NiO and MgO in the spinel solid solution. It was further noted that the Ni content of the bath in contact with the $Ni_{0.5}Mg_{0.5}Al_2O_4$ was more than six times lower than in contact with the pure $NiFe_2O_4$ whilst the content of Mg in the bath in contact with the spinel solid solution had the same order of magnitude as that of Ni from the $NiFe_2O_4$. Given the higher thermodynamic stability of MgO than NiO, the dissolved Mg may be less likely to be co-deposited with Al than the dissolved Ni. Furthermore, the $Ni_{0.5}Mg_{0.5}Al_2O_4$ solid solution is also more difficult to reduce by liquid Al compared to $NiFe_2O_4$ due to the reduced NiO activity in the spinel solid solution. Hence, $(Ni,Mg)Al_2O_4$ solid solutions could be potentially promising materials for the ledge-free HHC sidewalls when considering chemical resistances towards the baths and liquid Al.

Table II. The experimental conditions used for studying chemical and dissolution reactions in the spinels/bath system at 980 °C

Run No.	Specimen	Fabrication of Specimens		Corrosion Testing of Specimens				
		Sintering temp. (°C)	Sintering time (h)	Electrolyte (wt%)	Bath ratio	Time (h)	Rotation speed (rpm)	Atmosphere
1	As prepared melt of 90%cryolite/10%Al_2O_3	n.a.	n.a.	82%cryolite/10%Al_2O_3/ 3%AlF_3/5%CaF_2	1.38	0	0	CO_2
2	*$MgFe_2O_4$	1500	3	90%cryolite/10%Al_2O_3	1.50	24.00	25	Air
3	*$NiFe_2O_4$ [20]	1450	3	82%cryolite/10%Al_2O_3/ 3%AlF_3/5%CaF_2	1.38	24.00	24	CO_2
4	$NiAl_2O_4$	1500	6	82%cryolite/10%Al_2O_3/ 3%AlF_3/5%CaF_2	1.38	24.00 30.00 96.00	0	CO_2
5	$MgAl_2O_4$	1500	72	82%cryolite/10%Al_2O_3/ 3%AlF_3/5%CaF_2	1.38	6.08 24.25 31.25 48.38 55.38 127.05 151.12	0	CO_2
6	$Ni_{0.5}Mg_{0.5}Al_2O_4$	1500	72	82%cryolite/10%Al_2O_3/ 3%AlF_3/5%CaF_2	1.38	5.00 23.08 30.08 47.22 54.08	0	CO_2

Notes: (a) The well mixed oxides were uniaxially cold-pressed in hard steel dies under 120 MPa into green rectangular bars.
(b) * stands for the specimens that were dynamically tested in the stirred finger test apparatus. All others were statically tested in the cups containing the baths.

Table III. XRF analysis of some solidified baths after the corrosion tests at 980 °C

Run No.	Sample	Time (h)	Bath Ratio/ Atmosphere	Elemental Concentration (wt %)				
				Al	*Ni*	*Mg*	*Fe*	*Ca*
1	As prepared melt of 90%cryolite/10%Al_2O_3	0	1.5/air	18.6	<0.004	<0.01	0.056	0.52
2	*$MgFe_2O_4$	24	1.5/air	18.1	<0.004	0.38	1.57	0.48
3	*$NiFe_2O_4$ [20]	24	1.38/CO_2	18.1	0.045	0.05	0.16	3.05
4	$NiAl_2O_4$	24	1.38/CO_2	17.8	0.015	0.02	0.02	2.63
		30		17.4	0.01	0.02	0.02	2.66
		96		16.7	0.01	0.02	0.02	2.79
5	$MgAl_2O_4$	6.08	1.38/CO_2	16.4	<0.004	<0.01	0.01	2.72
		24.25		16.2	<0.004	<0.01	0.009	2.78
		31.25		16.2	<0.004	0.01	0.014	2.77
		48.38		16.0	<0.004	0.01	0.008	2.80
		55.38		16.0	<0.004	0.01	0.01	2.82
		127.05		15.6	<0.004	0.05	0.016	2.87
		151.12		15.4	<0.004	0.07	0.009	2.88
6	$(Ni_{0.5}, Mg_{0.5})Al_2O_4$	5.00	1.38/CO_2	16.9	0.027	0.02	0.02	2.68
		23.08		16.6	0.004	0.04	0.04	2.69
		30.08		16.5	0.007	0.05	0.01	2.67
		47.22		16.5	0.007	0.05	0.01	2.73
		54.08		16.4	<0.004	0.05	0.01	2.74

Notes: * stands for the specimens that were dynamically tested in the stirred finger test apparatus. All others were statically tested in the cups containing the baths.

Conclusions

In this study, aluminate spinels, i.e. $NiAl_2O_4$, $MgAl_2O_4$ and $Ni_{0.5}Mg_{0.5}Al_2O_4$, have been tested in cryolite-AlF_3-Al_2O_3-CaF_2 electrolyte melts at 980 °C under air and CO_2. The results indicated that both $NiAl_2O_4$ and $MgAl_2O_4$ had good corrosion resistances towards the melts under CO_2, with solubility of Ni from $NiAl_2O_4$ being 0.01wt% and Mg from $MgAl_2O_4$ being 0.07wt%. It was also shown in this study that the dissolutions of Ni and Mg could be reduced by employing the $(Ni,Mg)Al_2O_4$ solid solution (with Ni:Mg molar ratio of 1:1). It was suggested that this was due to reduced activities of NiO and MgO in the spinel solution. Further investigations need to be carried out for the detailed mechanisms of the dissolution of these spinels in electrolyte baths.

Acknowledgements

The authors thank CSIRO Light Metal Flagship and Swinburne University of Technology for the provision of funding.

References

1. K. Grjotheim and B.J. Welch, Aluminum Smelter Technology, Aluminium-Verlag GmbH, Dusseldorf, 1980.
2. B. Benkahla, O. Martin, and T. Tomasino, "AP50 performances and new development", *Light Metals 2009*, G. Bearne, ed., TMS, Warrendale, PA, (2009), pp. 365-370.
3. W.T. Choate and J.A.S. Green, "U.S. energy requirements for aluminum production: Historical perspective, theoretical limits and new opportunities", *prepared under Contract to BCS, Incorporated, Columbia, MD., U.S. Dept. Energy, Energy Efficiency and Renewable Energy*, Washington, D.C., 2003.
4. A.T. Tabereaux, "Reviewing advances in cathode refractory technology", *JOM*, 11 (1992), pp. 20-26.
5. G. Brooks, M. Cooksey, G. Wellwood, and G. Goodes, "Challenges in light metals production", *Mineral Processing & Extractive Metallurgy, TIMM C*, 116 (2007), pp. 25-33.
6. I. Galasiu, R. Galasiu, and J. Thonstad, Inert anodes for aluminium electrolysis, 1st ed., Aluminium-Verlag GmbH, Dusseldorf, 2009.
7. R.P. Pawlek, "Wettable cathodes: An update", *Light Metals 2010*, J.A. Johnson, ed., TMS, Warrendale, PA, (2010), pp. 377-382.
8. A.T. Tabereaux, "Silicon carbide bricks in aluminum reduction cell cathodes", *Light Metals Proc. And Appl.*, Canadian Inst. of Mining, (1993), pp. 149-163.
9. J. Keniry, "The economics of inert anodes and wettable cathodes for aluminum reduction cells", JOM, 53 (2001), pp. 43-47.
10. R. Mukhlis, M.A. Rhamdhani, and G. Brooks, "Sidewall materials for Hall-Heroult process", *Light Metals 2010*, J.A. Johnson, ed., TMS, Warrendale, PA, (2010), pp. 883-888.
11. R.P. Pawlek, "SiC in electrolysis pots: An update", *Light Metals 2006*, T.J. Galloway, ed., TMS, Warrendale, PA, (2006), pp. 655-658.
12. J. Schoennabl, E. Jorge, O. Marguin, S.M. Kubiak, and P. Temme, "Optimization of Si_3N_4 bonded SiC refractories for aluminum reduction cells", *Light Metals 2001*, J. L. Anjier, ed., TMS, Warrendale, PA, (2001), pp. 251-255.
13. E. Hagen, M.A. Einarsrud, and T. Grande, "Chemical stability of ceramic sidelinings in Hall-Heroult cells", *Light Metals 2001*, J.L. Anjier, ed., TMS, Warrendale, PA, (2001), pp. 257-263.
14. M.V. Swain and E.R. Segnit, "Reaction between cryolite and silicon carbide refractories", *J. Aust. Ceram. Soc.*, 20 (1984), pp. 9-12.
15. B.J. Welch and A.E. May, "Materials problem in Hall-Heroult cells", *8th Int. Leichmetalltag.*, Leoben-Vienna, (1987). pp. 120-125.
16. R.P. Pawlek, "Methods to test refractories against bath attack in aluminum electrolysis pots", *Aluminium*, 70 (1994), pp. 555-559.
17. B.L. Gao, Z.W. Wang, and Z.X. Qiu, "Corrosion tests and electrical resistivity measurement of SiC-Si_3N_4 refractory materials", *Light Metals 2004*, A.T. Tabereaux, ed., TMS, Warrendale, PA, (2004), pp. 419-424.
18. J.G. Zhao, Z.P. Zhang, W.W. Wang, and G.H. Liu, "Test method for resistance of SiC material to cryolite", *Light Metals 2006*, T.J. Galloway, ed., TMS, Warrendale, PA, (2006), pp. 663-666.
19. D.R. Sadoway, "Inert anodes for the Hall-Heroult: the ultimate materials challenge", *JOM*, 53 (2001), pp. 34-35.
20. X.Y. Yan, M.I. Pownceby, and G. Brooks, "Corrosion behavior of nickel ferrite-based ceramics for aluminum electrolysis cells, *Light Metals 2007*, M. Sorlie, ed., TMS, Warrendale, PA, (2007), pp. 909-913.
21. T.E. Jentoftsen, O.-A. Lorentsen, E.W. Dewing, G.M. Haarberg, and J. Thonstad, "Solubility of iron and Nickel oxides in cryolite-alumina melts", *Light Metals 2001*, J.L. Anjier, ed., TMS, Warrendale, PA, (2001), pp. 455-461.
22. C.W. Bale et al., *FactSage thermochemical software and databases*, CALPHAD, 2002, **26**: p.189-228.
23. J. Granfield and J. A. Taylor, "The impact of rising Ni and V impurity levels in smelter grade aluminium and potential control strategies", *Materials Science Forum* 630 (2010), pp. 129-136.
24. O-A. Lorentsen, "Behaviour of Nickel, Iron and Copper by application of inert anodes in aluminium production", Doctoral Thesis, Department of Materials Technology and Electrochemistry, Norwegian University of Science and Technology, Trondheim, 2000.
25. T.E. Jentoftsen, O.-A. Lorentsen, E.W. Dewing, G.M. Haarberg, and J. Thonstad, "Solubility of some transition metal oxides in cryolite-alumina melts: Part I. Solubility of FeO, $FeAl_2O_4$, NiO, and $NiAl_2O_4$", *Metall. Mater. Trans. B*, 33 (2002), pp. 901-908.